Astron. Astrophys. 364, 501–516 (2000)

ASTRONOMY
AND
ASTROPHYSICS

On the viewing angle to broad-lined radio galaxies

J. Dennett-Thorpe, P.D. Barthel, and I.M. van Bemmel

University of Groningen, Kapteyn Institute, 9700AV Groningen, The Netherlands

Received 8 September 2000 / Accepted 20 October 2000

Abstract. We address the nature of broad-lined radio galaxies, in particular their radio axis orientation, using new, matched resolution, dual frequency radio observations of a sample of twelve nearby broad-lined extragalactic 3C objects. Radio spectral index and depolarisation asymmetries indicate that these objects have a preferred orientation with respect to the observer. In addition, the spectral asymmetries are suggestive of lower Doppler factors in the broad-lined radio galaxies when compared to 3C quasars. This is in agreement with their optical properties, and leads to the conclusion that some objects are lower powered versions – at similar lines of sight – of the more distant quasars, whereas others are at larger angles to the line of sight.

1. Introduction

Under most current paradigms of active galactic nuclei, the broad emission lines seen in the optical spectra of such objects are due to emission originating in regions close to a supermassive black hole. Orientation-dependent unification schemes (e.g. Scheuer 1987, Barthel 1989) posit that at large viewing angles this broad-line region is obscured by optically thick material (a putative dusty torus). Within this scheme, radio-loud quasars have been proposed to represent favorably oriented narrow-lined radio galaxies.

Broad-lined radio galaxies (BLRGs) have both a visible host galaxy (hence their identification on optical images as galaxies) and broad lines in their spectra. On account of these broad emission lines, BLRGs can be considered to be aligned to the observer at similar angles to the line of sight as the quasar population. This assumption is often made in statistical investigations of radio galaxies and quasars which are concerned with orientation, obscuration and relativistic motion. There is indeed evidence that some BLRGs are at comparable angles to the lines of sight to quasars (e.g. superluminal motion in some BLRGs (Alef et al., 1996)) and that, statistically, they are closer to the line of sight than their narrow-lined counterparts (Hardcastle et al. 1998; Gilbert & Riley 1999). From an analysis of the radio properties of BLRGs in the 3CR sample, Hardcastle et al. (1998) argue that BLRGs are simply low-luminosity counterparts of quasars. In this picture, the objects are classified as BLRGs because of the combined effects of the lower luminosity of the AGN and the proximity to the host enabling the starlight to be clearly detected.

However, there are two lines of evidence arguing against the simple picture that all broad-lined radio galaxies are nearby, low-luminosity quasars. Tadhunter et al. (1998) detect BLRGs out to the redshift limit of their sample, thus overlapping with the quasars in redshift and power. This suggests a considerable range in the intrinsic luminosities of the broad-line AGN for a given redshift or radio power. The authors favour this explanation over the possibility that the BLRGs are simply partially obscured quasars, because of the large scatter seen in the correlation between radio and [OIII] luminosities. Secondly, BLRGs have been shown to be unusual in their FIR spectral energy distribution. Many BLRGs show a short wavelength FIR excess seen neither in NLRGs nor in quasars, which is presumably due to hot dust (Hes et al. 1995). In fact, the first BLRG studied by IRAS already displayed this hot dust component (Miley et al. 1984). Further work is underway to investigate how general this property is, using the ISO satellite (van Bemmel et al., in prep.).

Not all the broad-line radiation may be reaching us directly. Combining results from optical spectropolarimetry with information on dust-induced reddening, Cohen et al. (1999) suggest a continuous transition with increasing aspect angle from unobscured quasars to reddened BLRG to NLRG. This argues that the obscuring torus does not have a distinct edge (see also Baker 1997). Cohen et al. model the optical AGN radiation of BLRGs with contributions from both dust-reddened and dust-scattered quasar light. Corbett et al. (1998) find that broad-line emission may be scattered both from the inner wall of the postulated dust torus and from its polar regions by electrons or dust clouds distributed along the radio jet.

It therefore seems likely that both the luminosity of the AGN itself and its orientation play a role in whether an object is classified as a BLRG or a quasar. In this paper we address the relative importance of these effects using radio and other data. Determining the orientation of the BLRG axis will be essential to discriminate between the possibilities and determine the location and nature of the hot dust.

Send offprint requests to: J. Dennett-Thorpe
Correspondence to: jdt@astro.rug.nl; pdb@astro.rug.nl

In addition to the brightness asymmetries of the jets and hotspots, which are crude indicators of orientation (see e.g. Hardcastle et al. 1998), there are two other orientation indicators in the radio emission: depolarisation and hotspot spectral index asymmetries. Depolarisation asymmetries related to orientation of powerful classical double radio sources was first reported by Laing (1988) and Garrington et al. (1988). Using a sample of quasars and radio galaxies with one detected jet, these studies show that the jet side is generally less depolarised. This is most easily understood as an orientation effect, in which the jet is pointing towards us and the counterjet side is seen through a greater depth of depolarising material associated with the host galaxy.

Spectral asymmetries related to jet-sidedness in powerful radio sources with detected one-sided jets were first reported by Garrington et al. (1991). The observations in that paper were insufficient to ascertain if the asymmetry was due to the hotspot material, or the extended lobe material: a situation complicated by the detection of spectral asymmetries in the extended material in another sample (Liu & Pooley, 1991). Dennett-Thorpe et al. (1997; hereafter D97) addressed this issue and showed that the spectral asymmetries could be separated into two components: one in the lobe material related to the confinement of the radio lobe and a second, of interest here, in the hotspots due to relativistic effects. The spectral asymmetry of the hotspots has also been confirmed by Ishwara-Chandra & Saikia (2000).

In this paper we present results of dual frequency radio observations of BLRGs and quasars taken for the purpose of investigating their orientation by use of the spectral and depolarisation asymmetries. We present the observations and data analysis (Sect. 2) before presenting the results, also combined with the data from D97 and D99 (Sect. 3). In Sect. 4 we present modelling of the expected spectral asymmetries, also in the presence of lobe contamination, and analyse the observed asymmetries related to the object classification (BLRGs and quasars). We finally consider other evidence on the viewing angles to the individual broad-lined objects considered in this paper, using data from the literature in conjunction with our results.

Throughout this paper we use a Friedmann cosmology with H_0=65 km s^{-1}Mpc^{-1} and q_0=0.5. We use the convention $S \propto \nu^{-\alpha}$.

2. Sample selection, observations and data reduction

The sample was chosen to include all broad-lined 3C objects in the redshift interval $0.15 < z < 0.36$, which exceed 20 arcsec in angular size. The size criteria ensures that all sources will be resolved by the observations. The upper limit of the redshift range was chosen to include all objects commonly considered as broad-lined radio galaxies, whilst the lower limit corresponds to the upper redshift limit of the 3C radio galaxy sample of Dennett-Thorpe et al. (1999; hereafter D99). That investigation involved a similar analysis, and contained two broad-lined radio galaxies (3C 382 and 3C 390.3), which are also included in part of the present analysis.

The previous detection of a jet was not a criterion for inclusion in the sample. We observed both known quasars and objects catalogued as BLRG. We excluded the blazar 3C 273 from our sample. The quasar 3C 249.1, which falls in the redshift range of our sample, was not observed in this programme, but was observed by D97, and is included in our analysis. The properties of the sample are summarised in Table 1. In the first three columns we give the 3C and IAU names, and the identification as narrow-line object (N); broad-line galaxy (B); or quasar (Q) (see Sect. 2.1). The next three columns give fundamental source parameters: redshift, monochromatic radio power at 1.4 GHz and largest angular size. The rotation measure and side of any detected jet are given in the final columns.

The observations were taken with the NRAO VLA at 1.4 GHz in B array on 3 Oct 1999 and at 4.9 GHz in C array on 1 Dec 1998. The arrays were chosen to deliver matched uv coverage at the two frequencies, which is crucial for spectral work. All reductions were done in AIPS. The absolute flux density and position angle calibration was done using 3C286. Other nearby amplitude calibrators were interspersed throughout the run. In order to maximise uv coverage, each source was observed several times (typically 6, with some restrictions due to scheduling constraints) over a period of several hours. Typical observational parameters are listed in Table 2. Baseline solutions were applied in the conventional manner by observing the sources 0410+769 and 1400+621.

Due to telescope failure 3C 286 was not observed in the 1.4 GHz observations, but was observed two days later, together with sources 1400+621 and 3C 287.1. In this way the absolute flux density was tied to the non-variable CSO 1400+621, and the stability of the polarisation solutions over the intervening two days could be checked by imaging 3C 287.1. Comparison of the observations showed the position angle and percentage polarisation to be the same within $<$3% for both runs, indicating that, as expected, the telescopes were stable over this time interval.

Data for all sources were phase self-calibrated to convergence, and the final uniformly-weighted images were produced by cleaning to the noise with AIPS task IMAGR. Particular care was taken to ensure the resultant images were cleaned sufficiently deep: spectral index work is particularly sensitive to the erroneous flux densities that can arise by restoring the clean conponents (mJy per clean beam) onto an insufficiently cleaned image (with flux density measured in mJy per dirty beam). The polarisation images were corrected for Ricean bias using the conventional AIPS tasks for this purpose.

The 5 GHz images are presented in Appendix A. The experiment was designed to yield identical resolution at both frequencies, and has higher sensitivity at 5 GHz. As a result, the 1.4 GHz images are virtually identical and are not shown here.

2.1. Classifications

The classification of an object as a quasar or a radio galaxy has been done in the past by a number of different workers. We therefore checked several characteristics ourselves to ensure homo-

Table 1. Source properties

Name	IAU name	ID	redshift	log($P_{1.4GHz}$) (W Hz^{-1})	LAS (arcsec)	RM (rad m^{-2})	jet-side
3C 17	0035−024	B	0.220	26.11	45	+10±3	SE
3C 33.1	0106+729	B	0.181	25.62	240	−15±3	S
3C 61.1	0210+860	N	0.184	25.91	185	–	–
3C 93	0340+048	B	0.357	26.40	27	+9±2	N?
3C 109	0410+110	B	0.306	26.33	100	−16±2	S
3C 206	0837−120	Q	0.197	25.43	169	−105±7	E
3C 219	0917+458	B	0.174	25.99	180	−19±2	S
3C 234	0958+290	B	0.185	25.86	120	+42±1	NE
3C 246	1048−090	Q	0.344	26.10	83	+0±3	–
3C 287.1	1330+023	B	0.216	25.76	110	+1±2	W
3C 323.1	1545+210	Q	0.264	25.94	68	+14±0.4	S
3C 332	1615+324	B	0.152	25.34	90	+2±1	S
3C 381	1832+474	B	0.160	25.55	75	+25±1	N?

References
Redshifts: 3C 17: Schmidt (1965); 3C 33.1: Chambers et al. (1996); 3C 61.1: Lawrence et al.(1996); 3C 93: Hewitt & Burbidge (1989); 3C 109,219,234,332,381: Hewitt & Burbidge (1991); 3C 206: Ellingson et al. (1989); 3C 246: Schmidt & Green (1983); 3C 287.1: Dunlop et al. (1989); 3C 323.1: Marziani et al. (1996)
Radio power: Computed from White & Becker (1992), except 3C 206 & 3C 246 for which we used PKSCAT90 (Wright & Otrupcek 1990), and 3C 61.1 (Kühr et al. 1981).
RM: Simard-Normandin et al. (1981)
Radio maps: 3C 17: Morganti et al. (1999); 3C 33.1: http://www.jb.man.ac.uk/atlas/; 3C 61.1: Leahy & Perley (1991); 3C 93: Harvanek & Hardcastle (1998); 3C 109: Giovannini et al. (1994); 3C 219: Perley et al. (1980); Clarke et al. (1992); 3C 234: Burns et al. (1984); Hardcastle et al. (1997); 3C 287.1: Antonucci (1985); 3C 332: Fanti et al. (1987); 3C 381: Leahy & Perley (1991); Hardcastle et al. (1997); 3C 323.1: Bogers et al. (1994);

Table 2. Observation parameters

date	frequency (GHz)		bandwidth (Mhz)	typical scans per source	integration time (mins)	r.m.s. noise (mJy)
3 Oct 1998	1.4650	1.6650	25.0	6	45	0.4
1 Dec 1998	4.8351	4.8851	50.0	6	45	0.1

geneity of definition across the sample. Firstly we checked the Digitised Sky Survey (of the second generation POSS plates) for evidence of the host galaxy. We concluded 3C 246 and 3C 323.1 were clearly stellar, 3C 93, 3C 234, 3C 287.1 and 3C 109 had some evidence for host galaxy or surrounding nebulosity, whilst on the remainder the host galaxy was clearly seen. The E–O colours were compared using the APM (which had no information for 3C 33.1, 3C 61.1, 3C 206), as bluer colours indicate a more dominant AGN contribution. 3C 246 and 3C 323.1 (both PG quasars) were the bluest objects, followed by 3C 287.1, 3C 234, 3C 93 and 3C 17.

Spectral confirmation of the objects' broad emission lines for most objects came from spectra published in Eracleous & Halpern (1994) (see note on 3C 61.1 below). For 3C 33.1, 3C 219 and 3C 381 other references were used (referenced in Appendix B).

Notes on individual sources can be found in Appendix B. Here we bring attention to the fact that 3C 61.1 has been previously misidentified as a broad-line object. 3C 381, although also reported to have broad lines, has no published spectrum confirming this. 3C 234 is a well-known broad-line object: it has broad wings on the lines in its total intensity spectrum, but these are much more prominent in polarised light, indicating that the broad-line region is partially obscured. 3C 93 and 3C 109 have been subject to extensive studies which suggest their nuclear regions are reddened. In summary, for the analysis of the radio asymmetries, we consider 3C 206, 3C 246 and 3C 323.1 as quasars, and the other objects (except 3C 61.1) as BLRGs. We return to these definitions later.

3. Empirical results

As not all the objects have detected jets, it is not possible to analyse all sources in terms of jet/counterjet side directly. We therefore allocate sides A and B to the structure, as indicated in Column 2 of Table 3. Where possible this has been associated

with the jet side, such that side A corresponds to the jet side. The sources in which the jet-side is not known, or ambiguous, are: 3C 61.1, 3C 93, 3C 246 and 3C 381. In three of these cases we have assigned a jet-side based on some hints of jet-like features in our maps, or those referenced in Table 1, whilst for 3C 246 the assignment was arbitrary.

3.1. Spectral asymmetries

Table 3 summarises the results of the analysis of the radio asymmetries. Columns 3 & 4 give the spectral indices of the entire radio lobes, excluding the cores, but including the jets and hotspots. Columns 5, 6 & 7 give the spectral indices of the hotspots, and spectral difference calculated in the manner of D97. This method uses the brightest regions of the source and integrates the flux in this region in the images at both frequencies. Using this method we are able to compare directly with the results obtained in that paper. In Column 8 we present the spectral index difference calculated in the more conventional way of using a two-component fit to the maximum: a single Gaussian component and a zero-level and slope (AIPS task IMFIT), where the peak of the Gaussian component is used to calculate the spectral index of the hotspot. We see very good agreement between the different methods of calculation (i.e. Columns 7 & 8).

For 3C 17 there is no good fit to such a Gaussian model at this resolution. The strong jet which is apparent in the higher resolution images (Morganti et al. 1999) is unresolved in this object – the only source for which this is the case. Therefore the (presumably) flat spectrum jet emission contributes substantially to the calculated jet side spectral index, and is undoubtedly the cause of the large spectral asymmetry in this object.

3C 206 has a bright compact feature far from the end of the radio lobe on the counterjet-side. We have taken this to be the hotspot, because sites of dramatic jet disruption and jet 'termination' are difficult to distinguish both theoretically and observationally.

Errors on spectral indices are dominated by the absolute flux density calibration, which we take as 3%, given that good solutions were obtained for 3C 286. However, in comparison of spectral index differences in parts of a single source, this calibration uncertainty cancels out, leaving $<$1% error due to noise alone. Thus the spectral index *asymmetry* in the hotspot regions has an error $<$0.01 from this origin.

The results are presented in Fig. 1, which also includes the results of the 3CR radio galaxies and quasars from D97 and D99. Two broad-line radio galaxies, 3C 382 and 3C 390.3 were studied in D99: interestingly these had shown no detectable spectral asymmetry in the hotspot regions.

It can be seen that the narrow-line radio galaxies (open circles) show asymmetries in both senses: they are scattered evenly both above and below the dashed line, indicating that in some sources the jet side hotspot has a flatter spectrum, whilst in others its spectrum is steeper. The quasars and the broad-line radio galaxies on the other hand show a strong bias towards having a flatter jet side spectrum in the hotspot region: they fall above the dotted line. Considering only the broad lined objects presented in this paper, with detected jets and spectral asymmetries, 6/8 have detectably flatter jet side hotspots. The probability that at least this number have flatter jet side hotspots by chance is quite substantial (14%) but is strongly affected by small number statistics. Considering the combined results of this paper (objects with detected jets only), D97 and D99, we find that 9/11 quasars and 6/7 BLRGs have flatter jet side hotspot spectra. There are, in addition, 1 quasar and 2 BLRGs with the same counterjet and jet side spectral indices. The probabilty that at least 15/21 sources show flatter spectrum jetside hotspots by chance is 4%.

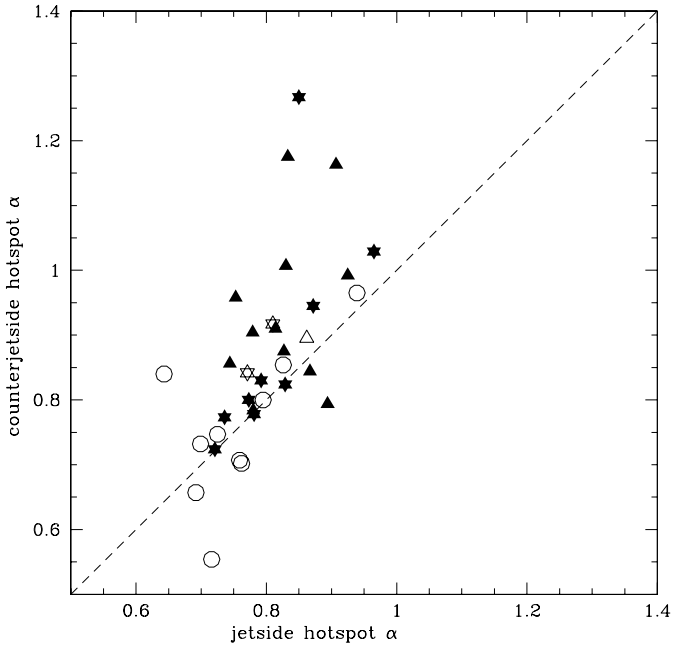

Fig. 1. Spectral indices of hotspots of BLRGs (stars), quasars (triangles) and narrow-line radio galaxies (open circles) in this paper combined with those in D97 and D99. BLRGs and the quasar with uncertain jet-sidedness are shown as open stars and triangle.

There is also a trend seen in Fig. 1 amongst the BLRGs and quasars that the magnitude of the asymmetry increases as the (mean) hotspot spectrum steepens. Fig. 2 shows the spectral asymmetry as a function of source redshift. If one excludes the insufficiently resolved source 3C 17 (z=0.22, $\Delta\alpha$=0.4), there is also a trend of increasing magnitude of asymmetry with redshift for the BLRGs and quasars.

3.2. Depolarisation asymmetries

We calculate the percentage polarisation,%P, of a radio lobe by integrating the flux density in the Ricean corrected polarised intensity image, above 5σ on the total intensity image (Columns 9 & 10 of Table 3). This is not the same as a single dish measurement, but has the advantage of allowing for changes in polarisation position angle across the source, as far as this has been resolved, without weighting towards the highly polarised boundary regions. The depolarisation parameter, DP, is calcu-

Table 3. Spectral and (de)polarisation properties.

source	side A	α_A	α_B	$\alpha_A^{\rm hs}$	$\alpha_B^{\rm hs}$	$(\alpha_B^{\rm hs}-\alpha_A^{\rm hs})$		$\%P_A^5$	$\%P_B^5$	DP_A	DP_B	DP_A/DP_B
3C 17	SE	0.81	0.89	0.85	1.27	0.42	–	06.5	07.9	0.355	0.329	1.08
3C 33.1	S	0.94	0.94	0.77	0.80	0.03	0.03	19.6	14.1	0.922	0.913	1.01
3C 61.1	N	1.03	0.98	0.94	0.96	0.03	0.03	24.2	16.1	0.269	0.297	0.91
3C 93	N	0.88	0.94	0.81	0.92	0.11	0.09	06.2	14.7	0.356	0.326	1.09
3C 109	S	0.94	0.94	0.87	0.94	0.07	0.08	12.1	12.3	0.314	0.308	1.02
3C 206	E	0.94	0.93	0.78	0.78	0.00	0.00	15.8	15.8	0.316	0.317	1.00
3C 219	S	1.02	1.02	0.79	0.83	0.04	0.04	14.7	15.8	0.292	0.304	0.96
3C 234	NE	1.00	1.03	0.96	1.03	0.06	0.06	15.9	12.7	0.289	0.283	1.02
3C 246	W	0.89	0.92	0.86	0.90	0.03	0.03	04.2	06.0	0.355	0.315	1.13
3C 287.1	W	0.81	0.84	0.83	0.82	-0.01	-0.01	12.8	13.0	0.360	0.346	1.04
3C 323.1	S	0.86	0.86	0.87	0.84	-0.02	-0.03	06.0	08.4	0.333	0.333	1.00
3C 332	S	0.86	0.88	0.74	0.77	0.04	0.03	16.3	13.4	0.338	0.328	1.03
3C 381	N	0.82	0.84	0.77	0.84	0.07	0.08	07.7	16.2	0.945	0.918	1.03

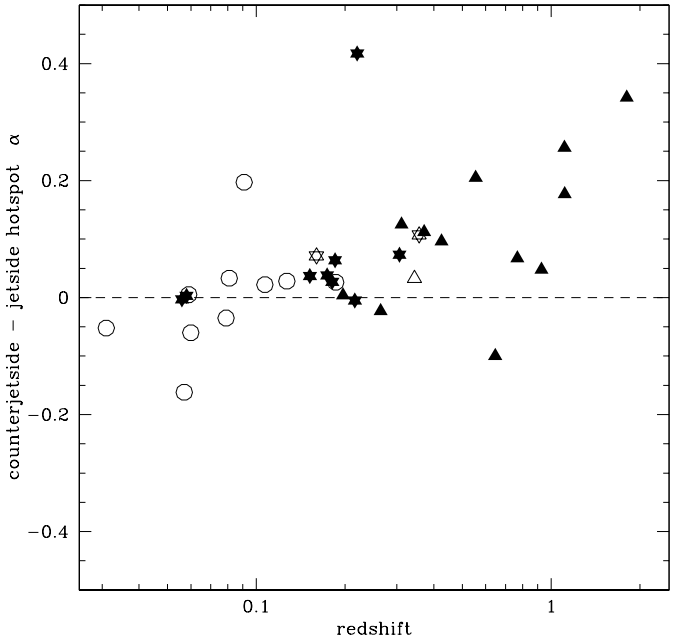

Fig. 2. Spectral asymmetries in hotspots of BLRGs (stars), quasars (triangles) and narrow-line radio galaxies (circles), (as Fig. 1) as a function of redshift.

lated as $\%P_{1.4}/\%P_5$ (Columns 11 & 12). The core has been excluded from these measurements, but not the jet. If side B (usually the counterjet side) is more heavily depolarised, the final column is > 1.

Errors in DP calculated from the noise on the maps alone are small, typically $\lesssim$1%. Absolute flux density calibration will not affect this quantity, but the polarisation calibration will. From inspection of the solutions obtained during the calibration procedure, we conclude that the fractional polarised flux densities are accurate to within 3%. We therefore take the errors on the depolarisation parameter to be $\sim$3%.

From inspection of Table 3, we see that 10 of the broad-lined objects (thus, excluding 3C 61.1) show an asymmetric depolarisation. Of these, 9 are more heavily depolarised on 'side B'. Taking the objects with known jet-sidedness only, we see that 6/7 sources have more depolarised counter-jet sides, in good agreement with the findings of Laing, Garrington et al. The probability that at least this number show this asymmetry by chance is 6%. The one source (3C 219) which shows depolarisation in the other sense, has a flatter jet side hotspot (i.e. does not have a spectral asymmetry counter to the expected sense). The NLRG 3C 61.1 has an ambiguous jet detection, but the side with the flattest hotspot and the least depolarisation are different, so cannot both indicate the jet side. This is expected for a source in the plane of the sky, as environmental effects are known to cause both spectral and polarisation asymmetries (D99 and references therein). Of the BLRGs and quasars with ambiguous or no jet detections, all have the depolarisation and spectral asymmetries in the sense that the least depolarised side is also the side with the flattest hotspot. We believe that, given the strength of the correlations where the jet side is known, we may use these asymmetries, and their consistency, to indicate jet side in all three of these sources. Thus these sources are marked in the figures which are labelled in terms of jet-sidedness. We have, however, clearly distinguished them (with open stars and triangles).

Fig. 3 shows the correlation of hotspot spectral index asymmetry and depolarisation asymmetry for the sources observations in this paper. Clearly most sources fall in the upper right quadrant where the hotspot region on the jet side has a flatter spectrum than on the counterjet side, and the jet side lobe is less depolarised. Excluding the NLRG 3C 61.1, we see that only 2/12 sources (3C 323.1 and 3C 219) fall well outside this quadrant.

4. Interpretation

4.1. Hotspot spectral asymmetries

The results of the preceding section showed that the BLRGs, like the quasars in D97, have, on average, flatter spectra on the jet side hotspots. This can be explained as an effect of relativistic Doppler boosting. The simplest explanation (Tribble, 1992) attributes this to a higher flux density of flat-spectrum hotspot

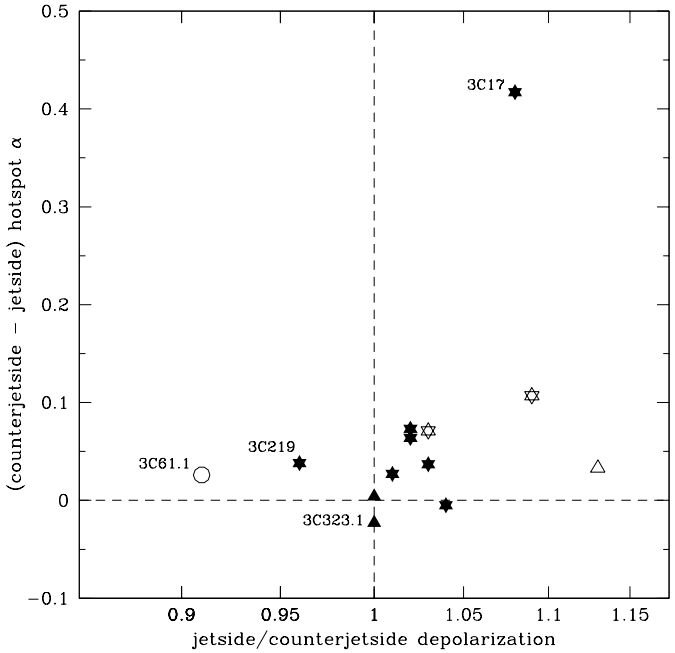

Fig. 3. Depolarisation and spectral asymmetries in hotspots of BLRGs (stars) and quasars (triangles) and 3C 61.1(circle) presented in this paper. Although all of the depolarisation asymmetries detected are marginally significant, for the entire sample of BLRGs and quasars both asymmetries are significant.

material on the jetted side, due to Doppler enhancement of this material over the quasi-stationary lobe material. This requires the jet side to have brighter hotspots at the resolution of the observations, whereas in fact only 5/12 of the quasars and 4/11 of the BLRGs (with known jet sidedness) show this effect. Thus, as argued in D97, the effect must be due to either Doppler frequency-shifting of curved hotspot spectra, or to Doppler suppression of the hotspot on the counterjet side.

The magnitude of the spectral asymmetry is smaller in the BLRGs than in the quasars (Fig. 1). This can be explained, to first order, as a result of the lower power/redshift of the BLRGs compared to the quasars. The interpretation of the spectral asymmetry arising due to a spectral curvature in the hotspot spectrum predicts such an effect with redshift, due to the shifting of the emitting frequencies for fixed observing frequencies. At higher redshift sources should have both steeper spectrum hotspots and greater spectral asymmetry due to this effect, as seen in Fig. 2. This effect was already apparent in D99. Analysis conducted in that paper showed that the higher emitted frequency observed in the higher redshift objects alone is insufficent to explain the magnitude of the effect, and therefore that part of the effect must be related to increasing radio power.

The notion of Doppler shifted curved spectra is well supported by the fact that the sources with steepest hotspot spectra have the highest spectral asymmetry (regardless of the power or redshift origin of this difference). In order to estimate the Doppler factors that would be required to produce the observed asymmetries, we assume a standard (curved) spectrum of the hotspots, and calculate the spectral asymmetry caused by a relativistic Doppler frequency shift. In this way the origin of the steeper spectra in higher power/ redshift objects is immaterial.

Fig. 4 illustrates both the effects on the observed spectra of changing the inclination to the line of sight θ, and the speed of the flow β. (It is the Doppler factor D(β, θ) which uniquely determines the curve, however as we are more interested in the angle to the line of sight we have presented the results in this form.) There are two families of curves, both for tangled magnetic fields, one for pitch-angle isotropised electron distributions (Jaffe-Perola (JP); solid line) the other for non-isotropised distributions (Kardashev-Pacholczyk (KP); dashed lines). The spectra due to isotropised electrons steepen increasingly with frequency, so the spectral asymmetry also increases with increasing mean spectral index (i.e. frequency). In the non-isotropised case however, there is a maximum asymmetry produced (as a function of mean spectral index, or observing frequency) as the spectrum at high frequency tends to (4/3)$\alpha_{\rm inj}$+1, where $\alpha_{\rm inj}$ is the low frequency (injection) spectral index. Continuous injection models result in lower asymmetries for a given Doppler factor and mean spectral index. We present only the KP/JP cases because these represent the extremes of possible spectra, and in particular the JP model yields strong lower limits on the Doppler factors required to produce the asymmetries. We have assumed an injection spectral index $\alpha_{\rm inj} = 0.7$. Other initial electron distributions, with power law indices, obviously have the effect of shifting the curves along the x-axis.

4.2. The effect of contamination by lobe material

So far we have assumed no contribution from underlying (non-boosted) material. The effect of such material – assuming this has a steeper spectrum than the hotspot material – is to increase the average observed spectral index of the hotspot region, but the effect on the spectral index asymmetry is complex, and depends on the assumed relative flux densities and spectra of the components. The effects are shown in Fig. 5 for two models of the lobe component, described below, for two different particle injection indices. In both cases an angle to the line of sight of 25° has been used, and the flow speed has been chosen to ensure the data points lie near the calculated loci (from inspection of Fig. 4).

We consider two models of the lobe material. One model (A) is given by $S_{\rm lobe} \propto \nu^{-1.5}$, and in the other model (B) the spectrum of the lobe material has the same spectrum as the hotspot material, but with the break frequency shifted to $0.1\nu_b^{\rm hs}$, where $\nu_b^{\rm hs}$ is the intrinsic break frequency of the hotspots. For each model take two different ratios of $S_{\rm hotspot}/S_{\rm lobe}$, satisfying the requirement that the hotspot remains detectable as such: the surface brightness of the hotspot is greater than that of the lobe material at a frequency $\sim 0.1\nu_b^{\rm hs}$.

We have plotted the results for the two models, in each case with (dotted lines) and without (dashed lines) the flux boosting of the hotspot taken into consideration. Although flux density boosting must occur if the hotspots contain relativistically moving material, other factors have been shown to determine the brightness of the hotspot, which is critical for the spectral asym-

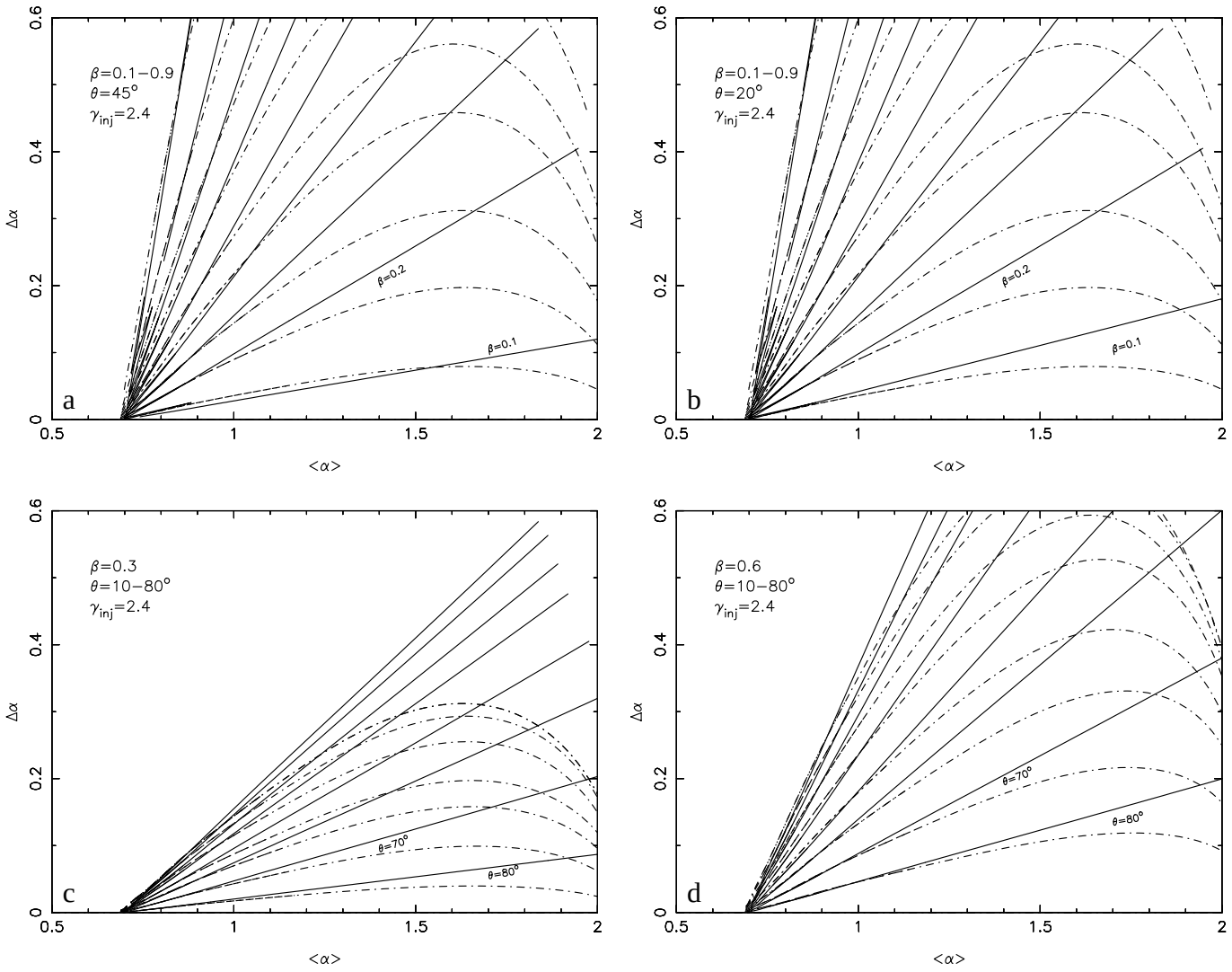

Fig. 4a–d. The spectral asymmetry as a function of average resultant spectral index for both JP (solid lines) and KP (dotted lines) cases. Results for motion inclined at **a** 45° and **b** 20° for β=0.1 to 0.9 (in steps of 0.1), and for **c** $\beta = 0.3$ and **d** $\beta = 0.6$ at angles to the line of sight ranging from 10° to 80° (in steps of 10°). No underlying continuum is assumed.

metry. We crudely illustrate this by neglecting the flux density boosting.

In summary, the effect of the inclusion of the lobe material is complex, and depends on both the spectral form of the lobe material and the relative brightness of the hospot to the background material. The effect will be to introduce considerable scatter into the observed hotspot spectral asymmetries. Therefore, we cannot use the spectral asymmetries as an accurate line of sight estimator for individual objects, unless our observations are of sufficiently high resolution to resolve the hotspots themselves, and thereby ascertain the contribution from the lobe material.

4.3. Comparison of BLRGs and quasars

In this section we assess whether there is any evidence from the spectral asymmetries for the BLRGs being statistically further from the line of sight. We define 3C 206, 3C 246 and 3C 323.1 as quasars and the remainder of broad-lined objects in the sample observed for this paper as BLRGs. We combine these with the BLRG and quasars from D97 and D99, as in the previous sections. Binning the data in average hotspot spectral index (Fig. 6), we see that the quasars show a greater increase in $\Delta\alpha$ with mean α (3C 17 has been excluded from this and following plots, and accompanying analysis on the grounds of obviously insufficient resolution.) From Fig. 4 we can see this could be explained by smaller Doppler factors (larger angles to the line of sight and/or smaller bulk jet speeds).

However, as the observations stand, there is the possibility of more lobe material in the 'hotspot region' of the BLRGs. We show in Fig. 7 our linear resolution of the observed sources as a function of redshift. We note that there is a group of predominantly BLRGs with < 30 beams across the source, which could be preferentially affected by lobe contamination. We therefore

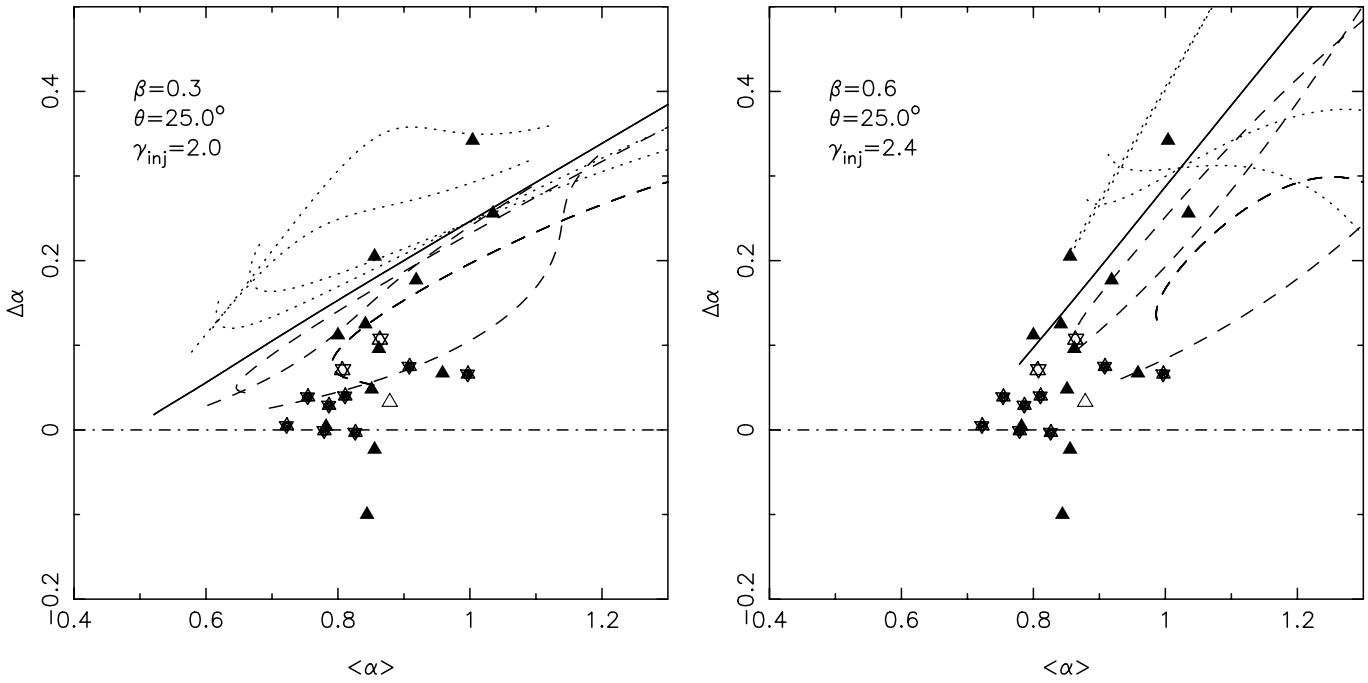

Fig. 5. The spectral asymmetry as a function of average resultant spectral index for the JP case, with inclusion of non-boosted lobe emission. Solid line shows zero unboosted (lobe) emission. The dotted and dashed lines refer to lobe emission plus Doppler frequency shifted hotspot emission, where the hotspot emission has also been Doppler boosted in flux density (dotted) or not (dashed). Lines tending to $\alpha_{\rm inj}$ (=$(\gamma_{\rm inj}-1)/2$; 0.5 left, 0.7 right) are model A, lines curving away from this are model B.

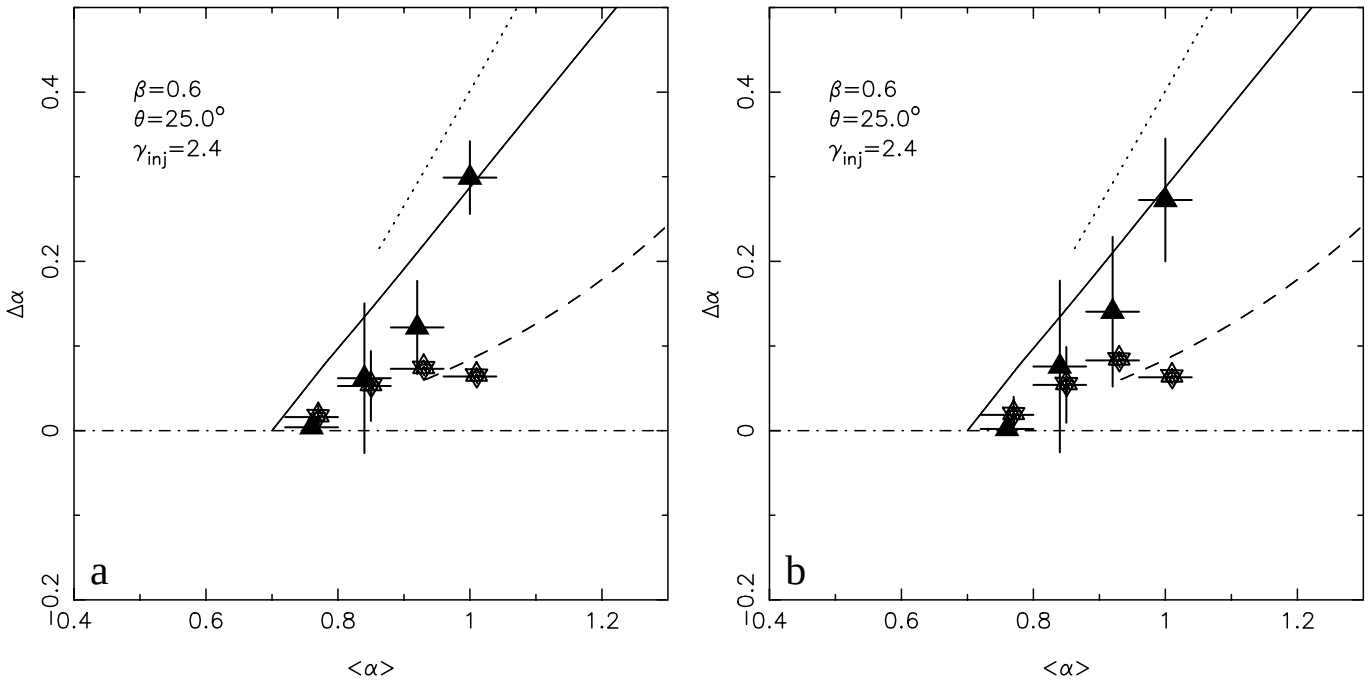

Fig. 6. The spectral asymmetries of the BLRGs (stars) and quasars (triangles) binned in mean spectral index of hotspots: **a** at original resolution and **b** at similar linear resolution (see text). The dotted and dashed lines indicate the effect of addition of background (lobe) material (model B, as before). Vertical error bars indicate spread in the measurements; horizontal error bars indicate the binning interval.

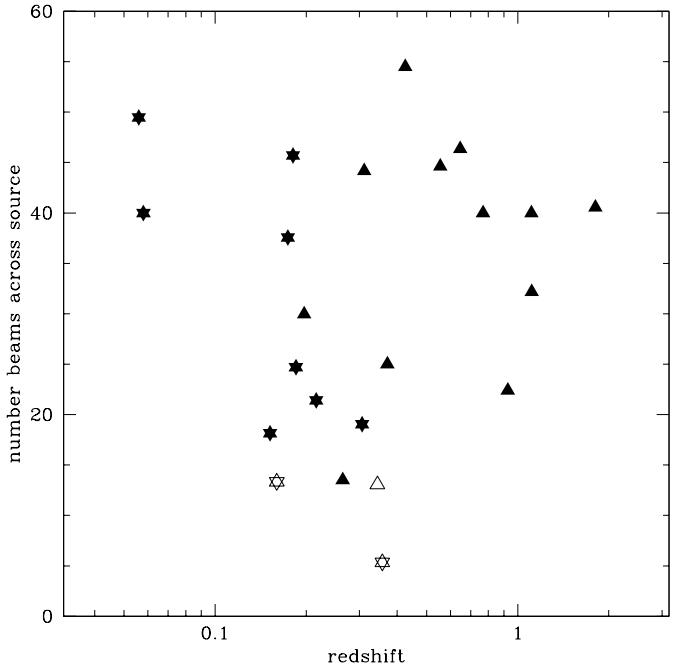

Fig. 7. The number of beams across the sources in the observations plotted in Fig. 6a.

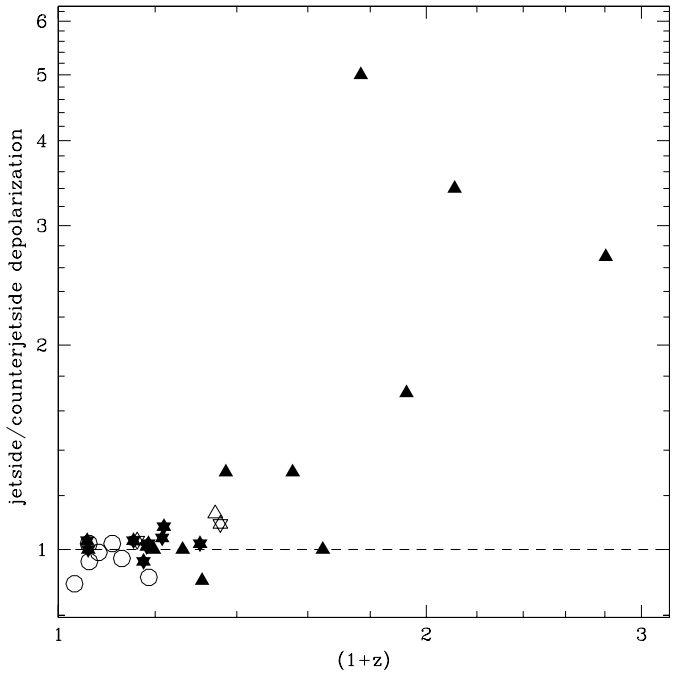

Fig. 8. Depolarisation asymmetries of the objects in this sample, together with data from D97 & D99. Symbols as Fig. 1

have convolved all the quasars and BLRGs of D97 and D99, and the BLRGs 3C 33.1 and 3C 219 from this paper to half the original resolution. The final distribution of linear resolution is then indistinguishable for the BLRGs and the quasars. From these images we derive the spectral asymmetry using the peak of a Gaussian fit to the hotspot. The results are plotted in Fig. 6(b), and are very similar to those in Fig. 6(a), showing that resolution effects are not the cause of the difference.

The BLRGs show a trend for smaller asymmetries at a given mean α. This difference is suggestive that the average Doppler factor in the hotspot material in the BLRGs may be smaller than the quasars. It is however, particularly dependent on the results from the BLRGs 3C 109 and 3C 234, which contribute the two BLRG points at high mean α.

We conclude that the observed spectral asymmetries are consistent with the BLRGs having moderately relativistic jet speeds ($\beta = 0.4 - 0.6$) and angles to the line of sight preferentially directed towards the observer. There is an indication of smaller asymmetries in the BLRGs which could be attributable to (some of the) the BLRGs in the sample having lower Doppler factors (i.e. larger angle to the line of sight, or smaller bulk speeds).

4.4. Depolarisation asymmetries

The depolarisation asymmetries in the BLRGs, like the spectral asymmetries, show the same sense but smaller magnitude compared to those in the quasars (D97) (Fig. 8). Again, the smaller magnitude of the effect may be attributed to power/ redshift as it is known that the depolarisation of radio sources increases with power/redshift (Kronberg et al., 1972; Leahy et al., 1986). Also, the magnitude of the asymmetry scales with strength of depolarisation, both observationally, and as expected by theory if the differential depolarisation is caused by differential lines of sight though a surrounding magneto-ionic halo (Garrington & Conway, 1991), or superdisk (Gopal-Krishna & Wiita, 2000). From the depolarisation properties we also conclude that in general the BLRGs are at similar angles to the line of sight as the quasars, but cannot rule out the possibility that some individual cases may be at larger angles.

5. Weaker or misdirected quasars?

As shown above, the scatter on the radio data means we are unable to determine the line of sight to individual objects in this manner. In an attempt to distinguish between objects which may be misdirected, or those which are intrinsically weaker with respect to their host galaxies, we consider other available evidence.

In Table 4 we present optical information from the literature for the 12 broad-line objects in the redshift-limited sample considered here. Although formally not members of the sample, the low redshift ($z = 0.06$) BLRGs 3C 382 and 3C 390.3 are also included. Firstly consider the starlight fraction of the sources with strong, unambiguous broad Hα lines. (Eracleous & Halpern, 1994, hereafter EH94) calculated the stellar contribution to their high resolution spectra, and these have been used where available as they represent by far the largest set of homogenous estimates of this type. However EH94's estimates are likely to be a lower limit to the stellar contribution, because the total galaxy is effectively underrepresented in a slit across the nucleus and host. Nonetheless,

as we shall see, useful information can be derived, despite the uncertainties.

We see that all objects classified as quasars in Sect. 2.1 have $<$10% stellar light, essentially confirming our independent classification. Of interest is the optical power of the AGN itself. First we will consider the AGN power (i.e. excluding the starlight) without adjusting for any intrinsic reddening (but taking Galactic extinction into account following Cardelli et al. 1989). The K-corrections are small and have been omitted. The resulting absolute magnitudes are listed in Column 6 of Table 4, and are denoted by M_{AGN}.

Before considering any reddening of the spectrum associated with absorption within the host galaxy, we can see that five sources (3C 93, 3C 109, 3C 206, 3C 246, 3C 323.1) may be considered as 'quasars' from their optical luminosity alone (using Schmidt & Green's (1983) cosmology adjusted $M< -22.4$ criterion). 3C 206, 3C 246 and 3C 323.1 were considered quasars by the criteria in Sect. 2.1, but 3C 93 and 3C 109 were not. As noted in Appendix B, 3C 109 is indeed an unusual object with apparently both high intrinsic reddening and a very blue underlying continuum. 3C 93 also has a highly reddened nucleus. In contrast, there is no evidence to suggest that 3C 206, 3C 246, 3C 323.1 are anything other than low redshift quasars: i.e. at similar lines of sight and with similar intrinsic powers as their higher redshift counterparts.

The remaining seven broad-lined sources whose M_{AGN} is below that for typical quasars include all of those whose lines show only 'broad wings'. For all of these latter objects there is no information about the percentage of the flux density due to starlight: but these all have optical appearances of galaxies so we can safely assume $<$ 50% of the observed light comes from the AGN. In this case $A_V \gtrsim 2$ would be required to bring these objects into the quasar luminosity range. We suggest that all these objects (if the broad wings on the spectral lines in 3C 381 are confirmed) are typically luminous quasars seen through the edge of the obscuring torus. X-ray observations and analysis are not available for all sources in this sub-sample, but there is good evidence for excess absorption towards 3C 219 (Sambruna et al., 1999). 3C 234 is probably the best candidate for an object at intermediate line of sight (see Appendix B).

Finally we consider the three sources which have strong, unambiguous broad lines, and are not the quasars discussed above (3C 17, 3C 332 and 3C 287.1). 3C 332 is a double peaked Hα emitter (EH94). 3C 93 is the only other such object in the sample. 3C 17 is also classified by EH94 as a 'disklike emitter' but has an asymmetric line profile which cannot be fitted with a simple disk model. It has a very large Hα FWHM (11500 km/s), less than the FWHM of the double peaked lines, but substantially more (at least a factor two) than all other objects in this sample. We do not fully understand how this class of objects fits into the orientation model. In order to become typically luminous quasars these three objects are also required to suffer reddening of their central continuum source (again typically $A_V \sim 2$). 3C 287.1 may be either an intrinsically weak quasar or seen through absorbing material: the available evidence is not clear.

Table 4. Optical source properties

Name	opt mag	A_V	M_{tot}	starlight fraction	M_{AGN}	ref
3C 17	18.02	0.077	–22.19	0.58	–21.25	EH94
3C 33.1	19.5	2.097	–22.29	–	–	
3C 93	18.09	0.804	–23.96	0.43	–23.35	EH94
3C 109	17.88	1.907	–24.92	$<$0.20	$<$–24.67	M81
3C 206	16.5	0.149	–23.04	0.00	–23.04	EH94
3C 219	17.22	0.059	–22.45	–	–	
3C 234	17.27	0.062	–22.54	0.35	–22.07	T95
				0.30	–22.15	M81
3C 246	16.00	0.144	–25.30	0.00	–25.30	EH94
3C 287.1	18.27	0.082	–21.91	0.36	–21.42	EH94
				0.50	–21.16	M81
3C 323.1	16.69	0.140	–24.00	$<$0.1	$<$–23.89	M81
3C 332	16.	0.079	–23.38	0.85	–21.32	EH94
3C 381	17.46	0.175	–22.13	–	–	
3C 382	14.73	0.23	–22.67	0.06	–22.60	EH94
3C 390.3	14.37	0.24	–22.97	0.31	–22.57	EH94

Optical magnitudes from Spinrad et al. (1985) for all sources but 3C 206 (a typical value from data presented in Ellingson et al., 1989: the source shows $\pm$1 mag variations) and 3C 246. A_V from NED. EH94=Eracleous & Halpern 1994; M81=Miller 1981; T95=Tran et al. 1995. 3C 382 and 3C390.3 were added for comparison – see text

Sambruna et al. (1999) report a surprising amount of absorption due to cold material in the ASCA spectra of *both* BLRGs and quasars. They differentiate between BLRGs and quasars on the basis of [OIII] luminosity. [OIII] luminosity is related to the intrinsic power of the source (Rawlings et al., 1989), and is believed to be isotropic to first order (Browne & Murphy 1987; Jackson & Browne 1991). However, there is strong evidence that some fraction of the [OIII] may be emitted in the obscured central regions (Jackson & Browne 1990; Hes et al. 1993). Therefore, while the division of Sambruna et al. is primarily by intrinsic power, it probably contains an additional orientation factor. We wish to divide the sources by orientation, so we reshuffle their objects into categories determined by the suggested orientations in this section. When classified in this manner, with 'BLRG' further from the line of sight, it appears that the BLRGs in the Sambruna et al. sample have significantly higher absorption column densities than the quasars, as expected.

In the light of these above considerations we divide the objects into the following categories.

IA – objects with strong broad lines, blue continuum, and a weak host 3C 206, 3C 246, 3C 323.1

IB – objects with strong broad lines, a clear but inconspicuous nucleus and prominent host galaxy: 3C 17, 3C 332

IIA – objects with strong broad lines, a prominent, reddened nucleus, and a relatively weak host: 3C 93, 3C 109, 3C 287.1

IIB – radio galaxies with a broad winged component in their spectra: 3C 33.1, 3C 219, 3C 234, 3C 381

These classifications are based on observational parameters, but divided with reference to simple, orientation dependent

models as follows. Category IA contains the normal quasars, whilst less luminous versions of these are found in IB. The well-known nearby BLRGs 3C 382 and 3C 390.3 are type I objects (both objects are optically variable Type 1 Seyfert nuclei). Their AGN luminosity makes them borderline IA/IB, but their low redshift makes their hosts conspicuous. Their starlight fraction estimated by EH94 is probably an underestimate, due to the effect of finite slit width.

Class IIA objects are probably seen at grazing incidence to the nuclear torus, with class IIB suffering more reddening and extinction due to intervening (torus?) dust. The difference between classes IIA and IIB may be a result of the optical AGN radiation of BLRGs being a composite of dust scattered and dust transmitted light (Cohen et al., 1999). Continued spectropolarimetry of BLRGs is crucial to address the validity of our classification in the framework of the Cohen et al. model. Whether or not Class II objects are at larger absolute angle to the line of sight than the quasars is dependent on the opening angle of the torus, which may exhibit large object to object variations, or may vary systematically with source power (e.g. Lawrence 1991; Hill et al. 1996).

We note with interest that the smaller Doppler factor required to explain the spectral asymmetries of the BLRGs compared to the quasars rests on two class II sources, namely 3C 234 and 3C 109. As there is good evidence that both these sources are observed at grazing angles to their tori, their jet Lorentz factors may still be in the range of objects in class IB (3C 234) and class IA (3C 109). In summary, in agreement with Cohen et al. (1999), we consider it likely that class II BLRGs are, *on average*, at larger angles than class IA quasars.

6. Conclusions

Analysis of continuum radio images at two frequencies of a carefully selected sample of broad lined radio galaxies and low redshift quasars, reveals asymmetries in both depolarisation properties and spectra of the hotspot regions. These asymmetries are generally associated with the side of the detected jet. These results are in the same sense as the asymmetries previously reported by Laing (1988), Garrington et al. (1988), Dennett-Thorpe et al. (1997, 1999), and can be understood as orientation effects: the depolarisation asymmetry as a line of sight effect, the spectral asymmetry as due to relativistic motion of the jet material on kiloparsec scales.

The sense of the asymmetries are consistent with the previous results, and reinforces the idea that the population of BLRGs is non-randomly oriented and that they are at close angles to the line of sight, similar to quasars. The magnitude of both the spectral and the depolarisation asymmetries is less than has been reported previously for the quasars. The smaller depolarisation asymmetry is explicable as a power/redshift effect. Sources at higher redshift in flux limited samples (i.e. also higher power) are known to depolarise more rapidly (Leahy et al., 1986), and thus the asymmetries are more pronounced.

The increasing spectral asymmetry with power/redshift may also be easily explained if the asymmetry is caused by relativistic Doppler effects in the hotspot material, if this has a curved spectrum. However, there is an indication of a difference in the magnitude of the spectral asymmetry between the classes of BLRGs and quasars, which is not a power/redshift effect, but could be explained by (some of) the BLRGs in the sample having lower Doppler factors (larger angle, or smaller bulk speeds) than the quasars. Although this result depends on just two sources, it is interesting to note that these two sources (3C 234, 3C 109) are the ones for which there is good evidence from other observations that they are viewed at grazing incidence to the torus.

As well as the problem of classification of objects by different workers in different manners, there is the additional problem that both the slightly 'misdirected quasars' and the lower power objects at lines of sight similar to the quasars are often classified, on observational grounds, as BLRGs. We have made comments on each individual source regarding its likely position in a physically based orientation scheme and consider that, whilst somewhat incomplete and uncertain, it is preferable to most subjective or arbitrary numerical decisions that are presently used.

In summary, this work supports the idea the object class of BLRGs is oriented preferentially towards our line of sight, and probably contains objects at somewhat larger angles than the quasar population, as well as less luminous quasars. The warm dust peak, detected in some of the BLRGs, has yet to be explained.

Acknowledgements. We are grateful to the staff of the VLA for assistance, and a rapid rescheduling of 3C 286. Thanks to Paul Alexander for the software which produced the spectra used to calculate the asymmetries. This research has made use of the NASA/IPAC Extragalactic Database (NED) which is operated by the Jet Propulsion Laboratory, California Institute of Technology, under contract with the National Aeronautics and Space Administration. The National Radio Astronomy Observatory is a facility of the National Science Foundation operated under cooperative agreement by Associated Universities, Inc. This research was supported by the European Commission, TMR Programme, Research Network Contract ERBFMRXCT96-0034 'CERES'.

Appendix A: radio images at 5 GHz

Appendix B: Notes on individual sources

3C 17 (PKS 0035−02) Morganti et al. (Morganti et al., 1999) show this morphologically peculiar source to contain a strong, bent jet on the south-eastern lobe. The Hα line has a strong broad component (EH94), and the nucleus shows optical polarisation (Tadhunter et al., 1997). Venturi et al. (2000) also find a VLBI jet in the same direction. De Koff et al. (1996, hereafter K96) show an HST image of the host which shows a 'compact nucleus'.

3C 33.1 The HST image (K96) shows a fairly undisturbed host galaxy. There is no published optical spectrum, but Laing et al. (1994) report broad wings on the Hα line.

3C 61.1 is a narrow-line galaxy, and was included erroneously in our original list. Lawrence et al. (1996) give a narrow-line spectrum for the western object in the triplet of galaxies. Giovanni et al. (1988) give a position for a radio core which

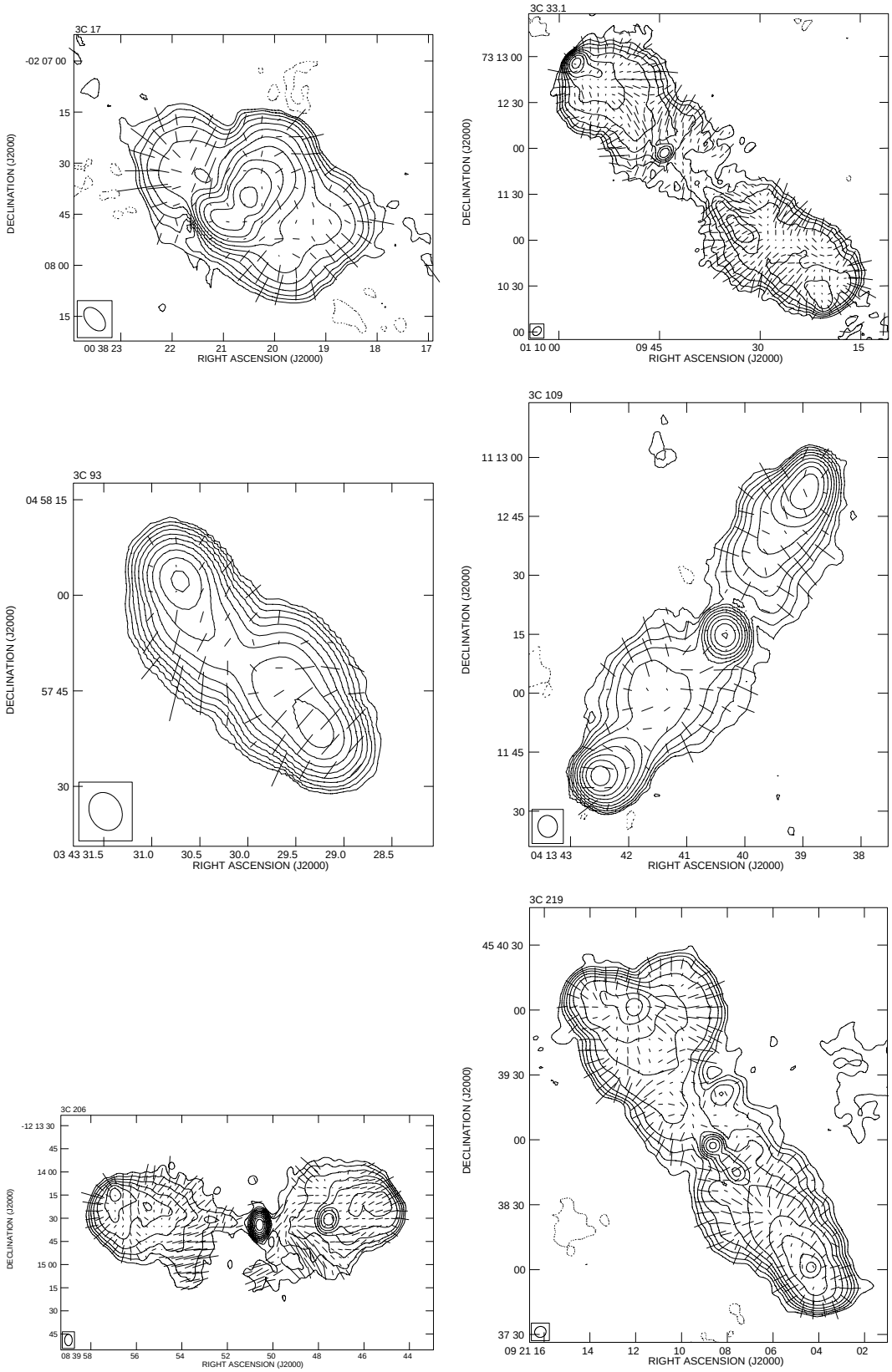

Fig. A.1. 5GHz (VLA in C array) images of the broad-lined objects in the sample. Contours are separated by factors of two in mJy/beam, with lowest contours $\pm$ 0.2 mJy/beam for 3C 33.1,3C 206,3C 219 and $\pm$ 0.4 mJy/beam for 3C 17,3C 93,3C 109. Vectors represent (RM uncorrected) apparent E-vectors with length proportional to fractional polarisation, such that 1 arcsec corresponds to 5% polarisation.

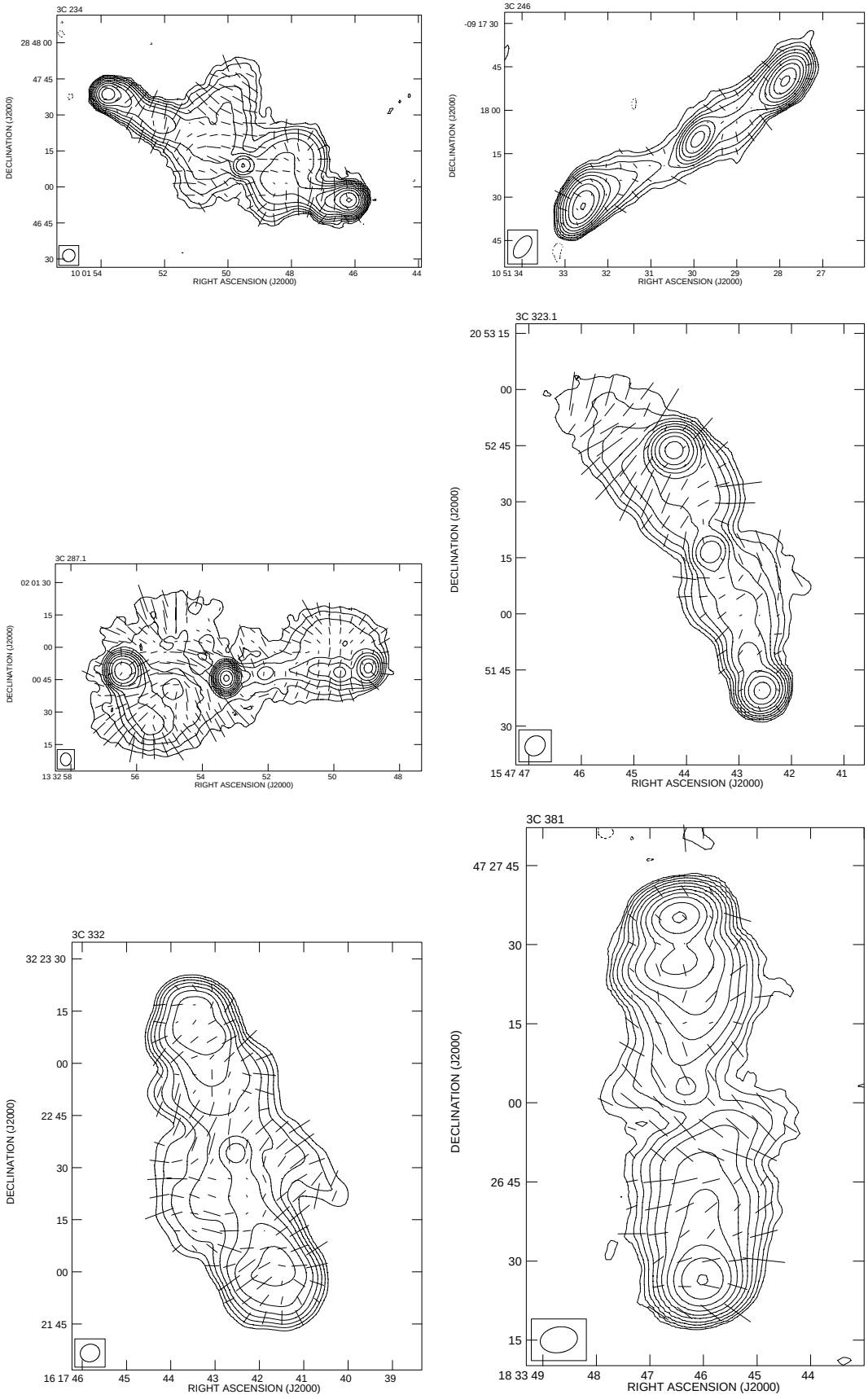

Fig. A.1. (continued)

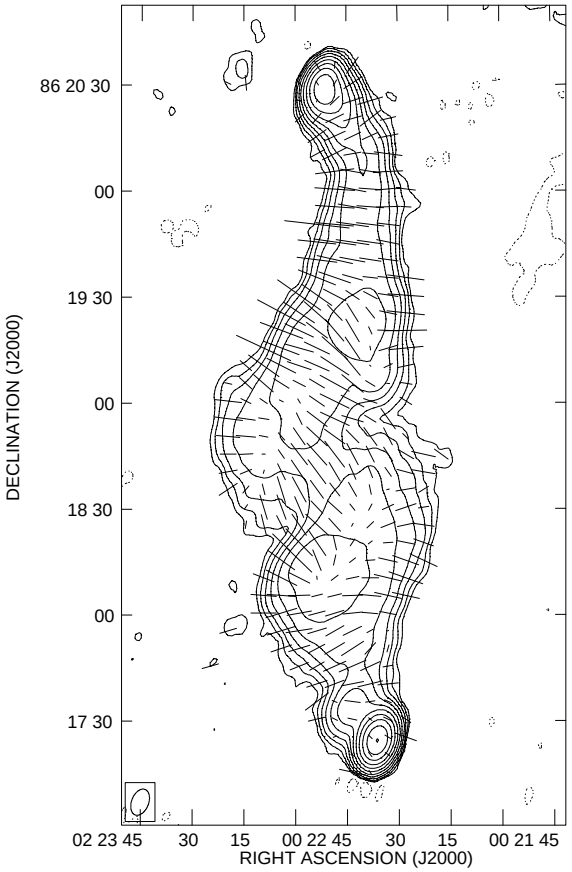

Fig. A.2. 5 GHz image of the narrow-line radio galaxy 3C 61.1 Contours are separated by factors of two in mJy/beam, with lowest contours $\pm$ 0.4 mJy/beam. Vectors as before.

falls on this galaxy. The BSO at the same redshift, identified by Penston (1971) and Miller, Robinson & Wampler (1973) falls outside the radio contours (Longair & Gunn (1975) give the finding charts). This source has lead to some confusion with 3C 61.1 appearing in lists of broad-lined objects. K96 note tails in the HST image of the host.

3C 93 This source has been classified as a BLLac due to the weak emission lines in the spectrum of Smith & Spinrad (1980), although it is now usually considered one of the nearest 3C quasars. It has very broad lines and is red (EH94). Hes et al. (1996) classify it as a BLRG due to its red colour and the slightly fuzzy R band continuum. EH94 derive a line of sight at $45\pm15^\circ$, based on disk models for the double-peaked Hα line profile.

3C 109 The nucleus is reddened ($A_V \sim 2.7$) (Rudy et al., 1984; Goodrich & Cohen, 1992; Rudy et al., 1999). De-reddening the nuclear source turns it into a typically luminous quasar (Goodrich & Cohen, 1992). Obscuring material is seen as excess absorption in the X-ray (Allen & Fabian, 1992; Allen et al., 1997). This source falls outside the simple two-component model for the optical emission (direct light plus scattered polarised light) of Cohen et al. (1999): it requires either excess absorption towards the BLR or an extra blue component in the continuum. Modelling the broad X-ray Fe line as emitted in the accretion disk, Allen et al. (1997) derive an inclination of $> 35^\circ$. The authors suggest that this object is at intermediate angle to the line of sight, grazing the torus. Giovanini et al. (1994) used the core/jet and jet/counterjet flux ratios to derive an angle to the line of sight of $34^\circ < \theta < 56^\circ$. A very compact nucleus and tails are seen on the HST images (K96). Taking the inferred intrinsic reddening into account Goodrich & Cohen (1992) determine $M_V < -26.6$

3C 206 is a fairly well-studied quasar. It is a member of a rich cluster (Ellingson et al., 1989), and shows optical variations of up to 2 mag in B. Ellingson et al. decompose the object into its host galaxy and non-thermal component and find: V=18.45; B$-$V=1.25 for host galaxy.

3C 219 displays narrow lines in the optical with broad wings on the Hα (1994). Fabbiano et al. (1986) report a strong Paschen-α line in the infra-red, and suggested this line was broad, a claim confirmed by Hill et al. (1996), who measured A_V=1.8$\pm$0.3. HST observations show a compact nucleus (K96). A strong jet is detected to the south (Perley et al., 1980; Clarke et al., 1992).

3C 234 shows both narrow and broad components in the Hα line, but only narrow components in the Hβ and higher Balmer lines (Grandi & Phillips, 1979). Some authors therefore refer to it as 'narrow line' (Taylor et al., 1996) and others 'broad line' (Carleton et al., 1984). Tran et al. (1995) show that most of the broad line flux is due to the polarised emission, with a very high (25%) intrinsic polarisation, and argue for scattering as the cause of the polarisation. It is optically variable (Miller, 1981). The BLR suffers heavy reddening, with an A_V calculated from Paα/Hα/Hβ line ratios of $\sim$2.4 (Carleton et al., 1984; Hill et al., 1996). High column densities are also detected in the X-ray (Sambruna et al., 1999). 3C 234 would therefore seem, like 3C 109, to be a good candidate for an object at intermediate angles to the line of sight. Tails are seen in the HST image (K96). Applying corrections for reddening and starlight contamination, Tran et al. (1995) derive $M_V \lesssim -24.2$, i.e. well within the range of typical quasars.

3C 246 (PKS 1048$-$090, PG1048$-$090) This object is also a member of the Bright Quasar Survey (Schmidt & Green, 1983; Green et al., 1986), so has been extensively studied at optical wavelengths. It is also a member of a cluster (Yates et al., 1989). No jet has yet been detected, but the source is not a member of the LRL sample, and has been relatively poorly imaged in the radio, in comparison with many other of the sources (Hutchings et al., 1998; Kellermann et al., 1994).

3C 287.1 The HST image shows a compact nucleus, as well as a second compact region to the W, less than 1kpc away (K96). A strong jet to the west, first indicated in Antonucci (1985), confirmed in Harvanek & Hardcastle (1998), is also clearly seen in our images. Analysis of the RASS data shows 3C 287.1 was detected with a photon index of $\approx$ 1.86 (Siebert et al., 1998), which is a value in the 'overlap region' between quasars and radio galaxies. Crawford & Fabian (1995) show the source has excess soft X-ray absorption.

3C 323.1 (PG1545+210) This has been a target for imaging investigations of the host galaxies of quasars (e.g. Stockton 1982). Miller (1981) concluded that the host galaxy must contribute $< 10\%$ of the optical light. Imaging with the HST has now detected its 'low surface brightness elliptical' (Bahcall et al., 1997). Boroson & Oke (1984) showed that the 'nebulosity' surrounding the quasar is highly ionised.

3C 332 The HST image shows a 'smooth elliptical nuclear region' (K96). It appears to be a member of a close pair. Halpern (1990) suggests this object as the prototype for relativistic accretion disk emission in the double-peaked Hα line, and EH94 derive a line of sight of $36\pm3^\circ$ based on fitting disk models to the profile of this line.

3C 381 A compact nucleus and tails appear in the HST image (K96). Grandi & Osterbrock (1978) claim 'a broad weak component of Hα', but to our knowledge there is no published spectrum of Hα to date. We suggest that its identification as a genuine BLRG may be open to doubt: it has no detected radio jet, and, unlike all other BLRG observed by Lilly & Longair (1982) its K band flux density is not higher than the NLRG in the sample.

References

Alef W., Wu S.Y., Preuss E., Kellermann K.I., Qiu Y.H., 1996, A&A 308, 376
Allen S.W., Fabian A.C., 1992, MNRAS 258, 29
Allen S.W., Fabian A.C., Idesawa E., et al., 1997, MNRAS 286, 765
Antonucci R.R.J., 1985, ApJS 59, 499
Bahcall J.N., Kirhakos S., Saxe D.H., Schneider D.P., 1997, ApJ 479, 642
Baker J.C., 1997, MNRAS 286, 23
Barthel P.D., 1989, ApJ 336, 606
Bogers W.J., Hes R., Barthel P.D., Zensus J.A., 1994, A&AS 105, 91
Boroson T.A., Oke J.B., 1984, ApJ 281, 535
Browne I.W.A., Murphy D.W., 1987, MNRAS 226, 601
Burns J.O., Basart J.P., de Young D.S., Ghiglia D.C., 1984, ApJ 283, 515
Cardelli J.A., Clayton G.C., Mathis J.S., 1989, ApJ 345, 245
Carleton N.P., Willner S.P., Rudy R.J., Tokunaga A.T., 1984, ApJ 284, 523
Chambers K.C., Miley G.K., van Breugel W.J.M., et al., 1996, ApJS 106, 247
Clarke D.A., Bridle A.H., Burns J.O., Perley R.A., Norman M.L., 1992, ApJ 385, 173
Cohen M.H., Ogle P.M., Tran H.D., Goodrich R.W., Miller J.S., 1999, AJ 118, 1963
Corbett E.A., Robinson A., Axon D.J., Young S., Hough J.H., 1998, MNRAS 296, 721
Crawford C.S., Fabian A.C., 1995, MNRAS 273, 827
de Koff S., Baum S.A., Sparks W.B., et al., 1996, ApJS 107, 621 (K96)
Dennett-Thorpe J., Bridle A.H., Scheuer P.A.G., Laing R.A., Leahy J.P., 1997, MNRAS 289, 753 (D97)
Dennett-Thorpe J., Bridle A.H., Laing R.A., Scheuer P.A.G., 1999, MNRAS 304, 271 (D99)
Dunlop J.S., Peacock J.A., Savage A., et al., 1989, MNRAS 238, 1171
Ellingson E., Yee H.K.C., Green R.F., Kinman T.D., 1989, AJ 97, 1539
Eracleous M., Halpern J.P., 1994, ApJS 90, 1 (EH94)
Fabbiano G., Willner S.P., Carleton N.P., Elvis M., 1986, ApJ 304, L37
Fanti C., Fanti R., de Ruiter H.R., Parma P., 1987, A&AS 69, 57
Garrington S., Conway R., 1991, MNRAS 250 198
Garrington S., Leahy J., Conway R., Laing R., 1988, Nat 331, 147
Garrington S.T., Conway R.G., Leahy J.P., 1991, MNRAS 250, 171
Gilbert G.M., Riley J.M., 1999, MNRAS 309, 681
Giovannini G., Feretti L., Gregorini L., Parma P., 1988, A&A 199, 73
Giovannini G., Feretti L., Venturi T., et al., 1994, ApJ 435, 116
Goodrich R.W., Cohen M.H., 1992, ApJ 391, 623
Gopal-Krishna, Wiita P.J., 2000, ApJ 529, 189
Grandi S.A., Osterbrock D.E., 1978, ApJ 220, 783
Grandi S.A., Phillips M.M., 1979, ApJ 232, 659
Green R.F., Schmidt M., Liebert J., 1986, ApJS 61, 305
Halpern J.P., 1990, ApJ 365, L51
Hardcastle M.J., Alexander P., Pooley G.G., Riley J.M., 1997, MNRAS 288, 859
Hardcastle M.J., Alexander P., Pooley G.G., Riley J.M., 1998, MNRAS 296, 445
Harvanek M., Hardcastle M.J., 1998, ApJS 119, 25
Hes R., Barthel P.D., Fosbury R.A.E., 1993, Nat. 362, 326
Hes R., Barthel P.D., Hoekstra H., 1995, A&A 303, 8
Hes R., Barthel P.D., Fosbury R.A.E., 1996, A&A 313, 423
Hewitt A., Burbidge G., 1989, A New Optical Catalogue of Quasi-stellar sources
Hewitt A., Burbidge G., 1991, ApJS 75, 297
Hill G.J., Goodrich R.W., Depoy D.L., 1996, ApJ 462, 163
Hutchings J.B., Dewey A., Chaytor D., et al., 1998, PASP 110, 111
Ishwara-Chandra C.H., Saikia D.J., 2000, MNRAS 317, 658
Jackson N., Browne I.W.A., 1990, Nat 343, 43
Jackson N., Browne I.W.A., 1991, MNRAS 250, 414
Kellermann K.I., Sramek R.A., Schmidt M., Green R.F., Shaffer D.B., 1994, AJ 108, 1163
Kronberg P., Conway R., Gilbert J., 1972, MNRAS 156, 275
Kühr H., Witzel A., Pauliny-Toth I.I.K., Nauber U., 1981, A&AS 45, 367
Laing R., 1988, Nat 331, 149
Laing R.A., Jenkins C.R., Wall J.V., Unger S.W., 1994, In: Bicknell G.V., Dopita M.A., Quinn P.J. (eds.) The First Stromlo Symposium. ASP Conference Series Vol. 54, p. 201
Lawrence A., 1991, MNRAS 252, 586
Lawrence C.R., Zucker J.R., Readhead A.C.S., et al., 1996, ApJS 107, 541
Leahy J.P., Perley R.A., 1991, AJ 102, 537
Leahy J., Pooley G., Riley J., 1986, MNRAS 222, 753
Lilly S.J., Longair M.S., 1982, MNRAS 199, 1053
Liu R., Pooley G., 1991, MNRAS 249, 343
Longair M.S., Gunn J.E., 1975, MNRAS 170, 121
Marziani P., Sulentic J.W., Dultzin-Hacyan D., Calvani M., Moles M., 1996, ApJS 104, 37
Miley G., Neugebauer G., Soifer B.T., et al., 1984, ApJ 278, L79
Miller J.S., 1981, PASP 93, 681 (M81)
Miller J.S., Robinson L.B., Wampler E.J., 1973, ApJ 179, L83
Morganti R., Oosterloo T., Tadhunter C.N., et al., 1999, A&AS 140, 355
Penston M.V., 1971, ApJ 170, 395
Perley R.A., Bridle A.H., Willis A.G., Fomalont E.B., 1980, AJ 85, 499
Rawlings S., Saunders R., Eales S.A., Mackay C.D., 1989, MNRAS 240, 701

Rudy R.J., Schmidt G.D., Stockman H.S., Tokunaga A.T., 1984, ApJ 278, 530
Rudy R.J., Puetter R.C., Mazuk S., 1999, AJ 118, 666
Sambruna R.M., Eracleous M., Mushotzky R.F., 1999, ApJ 526, 60
Scheuer P., 1987, In: Zensus J., Pearson T. (eds.) Superluminal radio sources. C.U.P., Cambridge, p. 104
Schmidt M., 1965, ApJ 141, 1
Schmidt M., Green R.F., 1983, ApJ 269, 352
Siebert J., Brinkmann W., Drinkwater M.J., et al., 1998, MNRAS 301, 261
Simard-Normandin M., Kronberg P.P., Button S., 1981, ApJS 45, 97
Smith H.E., Spinrad H., 1980, PASP 92, 553
Spinrad H., Marr J., Aguilar L., Djorgovski S., 1985, PASP 97, 932
Stockton A., 1982, ApJ 257, 33
Tadhunter C.N., Dickson R., Morganti R., Villar-Martin M., 1997, In: Clements D.L., Perez-Fournon I. (eds) Quasar hosts. Proceedings of the ESO-IAC Conference Tenerife, Spain, Springer-Verlag, p. 311
Tadhunter C.N., Morganti R., Robinson A., et al., 1998, MNRAS 298, 1035
Taylor G.L., Dunlop J.S., Hughes D.H., Robson E.I., 1996, MNRAS 283, 930
Tran H.D., Cohen M.H., Goodrich R.W., 1995, AJ 110, 2597 (T95)
Tribble P.C., 1992, MNRAS 256, 281
Venturi T., Morganti R., Tzioumis A., Reynolds J., 2000, A&A accepted
White R.L., Becker R.H., 1992, ApJS 79, 331
Wright, A., Otrupcek, R., 1990, Parkes Catalogue. ATNF
Yates M.G., Miller L., Peacock J.A., 1989, MNRAS 240, 129